Chapter 21

Segmented Foot with Compliant Actuators and Its Applications to Lower-Limb Prostheses and Exoskeletons

Qining Wang, Jinying Zhu, Yan Huang, Kebin Yuan and Long Wang

Additional information is available at the end of the chapter

http://dx.doi.org/10.5772/51495

1. Introduction

In recent years, there has been an increasing interest in the functionality of the foot in human normal walking. Different from the existing methods that represent the foot as a single rigid bar, several multi-segmented foot models have been studied to evaluate the effects of the segmented foot structures on human walking for clinical applications [1], adolescent gaits [2] and pediatric gaits [3]. The results show that the segmented foot with a toe joint has several advantages compared to the rigid foot in: walking step, walking speed, range of joint angle, change in angular velocity and joint energy-output. In addition, biomechanical studies conducted on ten donated limbs [4] indicate that the human foot can not be considered as a single rigid body with no intrinsic motion.

Inspired by biological investigations, several studies implemented segmented feet in robotic systems to improve walking performance. One of the main applications is in humanoid robots. Simulations and experiments on prototypes showed that adding toe joints could increase the walking speed of biped robots [5, 6]. These works were carried on humanoid robots based on the trajectory-control approach [7]. By controlling joint angles precisely, the robots can achieve static equilibrium postures at any time during motion. However, this kind of bipedal walking features low resemblance to human normal gaits and high energy consumption [8]. In contrast to the active-control bipedal walking mentioned above, passive dynamic walking [9] has been developed as a possible explanation for the efficiency of the human gait. Investigations on the effects of segmented foot, which are based on passivity-based model, may reveal more insights on real human walking. Though several efforts have been made in adding flat feet to passivity-based models [10–15], only a few studies have investigated passive dynamic bipedal walking model with segmented feet. Recently, [16] proposed a passive dynamic walking model with toed feet. Specifically, in the work, the authors contributed to the investigation of the passive bipedal walking behavior under toe joint rotation. The toe-rotation phase is initiated by ankle-strike. Simulation results showed that the advantages of the proposed walker come from its relation to arc-feet walker.

However, the effects of heel-strike and toe-strike during normal walking are ignored, which may influence the characteristics of bipedal walking [12]. In addition, the phase of rotation of the stance foot about the toe tip is ignored in this model, which makes the bipedal walking gait far from natural human-like gait.

Another area that can use segmented foot is rehabilitation robotics, e.g. lower-limb prostheses and exoskeletons. Although foot prosthesis was invented thousands of years ago, the development of foot prostheses is not as fast as people expect. Most of today's commercial foot prosthesis are passive and do not comprise segmented foot. In 1998, [17] first built a powered ankle-foot prosthesis which was powered by a pneumatic actuator. Then, several pneumatic actuated prostheses have been developed [18, 19]. Though the pneumatic actuator is lightweight, inherently compliant and capable of generating high forces, its control difficulties, large size and noise restrain the development of pneumatic driven prosthesis. Recently, [20] developed a powered ankle-foot prosthesis driven by a DC motor. The motor implemented compliant actuation and was placed on the ankle joint. The prosthesis can provide net positive work to propel the body upward and forward during the stance period. Experimental results show that the prosthesis can decrease the amputee's metabolic cost by 14% on average as compared to the conventional passive-elastic prosthesis. However, the prosthesis functionality is not comparable to that of the human foot because of the absence of segmented foot with toe joint. Similarly, although exoskeletons were invented several decades ago [21], there is no powered toe joint implemented in existing exoskeleton systems, e.g. [22, 23].

In this chapter, we discuss the effects and applications of adding segmented feet with compliant joints to lower-limb prostheses and exoskeletons. To analyze the effects of segmented foot and compliant joints on energetic efficiency and stability of bipedal walking, we first propose a passivity-based dynamic bipedal model which shows resemblance to human normal walking. Phase switching is determined by the direction of ground reaction force. The push-off phase includes rotation around toe joint and rotation around toe tip, which show a great resemblance to natural human gait. The effects of foot structure on motion characteristics including energetic efficiency and walking stability is investigated through simulation experiments. Starting from the theoretical analysis, we introduce segmented foot with toe joint in both ankle-foot prosthesis and exoskeleton prototypes. Both the ankle and toe joints are driven by two series-elastic actuators (SEA), which not only provide the required torque, but also shock tolerance and energy storage during walking. Preliminary studies on sensory based feedback control are carried out to improve the movement of the proposed systems. Experimental results validate the effectiveness of the proposed structure and actuation method.

The rest of the chapter is organized as follows. In section 2, we introduce the idea of adding segmented feet with compliant actuators placed on ankles and toes. Specifically, a theoretical model with segmented feet is proposed which is based on the simplest walking model. In Section 3, detailed investigations are presented to analyze the effects of segmented foot with joint compliance on dynamic walking. Then, starting from the theoretical analysis, the applications of segmented feet to lower-limb prostheses and exoskeletons are introduced in Section 4. After an overview of current compliant actuators in robotics, the development of a lower-limb prosthesis and an exoskeleton with powered compliant ankle and toe joints is presented. In section 5, the basic control method and related experiments on the prototypes are described. Experimental results validate the effectiveness of the proposed systems.

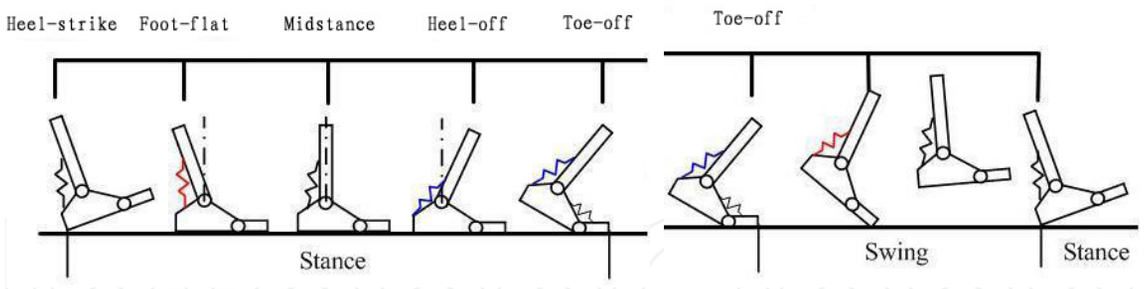

(a) Stance phase (b) Swing phase

Figure 1. One typical gait cycle. Each cycle includes two main subdivisions: (a) stance phase, (b) swing phase. The four important instants in every cycle are heel-strike (HS), foot-flat (FF), heel-off (HO) and toe-off (TO).

2. Dynamic walking model

2.1. Human normal walking gaits

Human walking is a cyclic pattern of bodily movements that is repeated over and over, step after step. Every gait cycle starts with heel-strike (HS) when the heel initially touches the ground and ends with the next HS of the same leg. As shown in Fig. 1, each cycle can be divided into two main phases: stance phase and swing phase [44]. The stance phase begins at the moment of HS and ends at the moment of toe-off (TO) when the forefoot pushes off the ground. The swing phase begins at the moment TO and ends at the next HS. The stance phase takes up 60% of the gait cycle and includes four subphases: 1) Hs to foot-flat (FF); 2) FF to midstance (MS); 3) MS to heel-off (HO); 4) HO to TO.

As introduced in [44], at the moment of HS, the ankle has to endure the impact force when the heel initially contacts the ground. From HS to FF, the ankle stores elastic energy within plantarflexor muscles. During FF to MS, the energy stored during the preceding period is released to help the body change the center of gravity from the support leg to the foreleg. At MS, the ankle begins to store elastic energy to dorsiflexor muscles and at HO the ankle reaches a state of maximum dorsiflexion. Then in the period HO to TO, ankle releases the energy stored in the last period to propel the body. However, the stored energy is much less than the energy needed. Then the ankle has to output much more net positive work. Meanwhile, the forefoot is bent to store energy. At the end of the period HO to TO, the toe joint releases the stored energy and supplements some net work to propel the body. During swing phase, the main function of the ankle and toe joints is to adjust the position of the foot to prepare for the next stance phase.

2.2. Bipedal model

To further investigate the effects of compliant joints and segmented feet on dynamic bipedal walking, in this section, we propose a passivity-based dynamic bipedal walking model that is more close to human beings. In the model, compliant ankle joints and flat segmented feet with compliant toe joints are included. As shown in Fig. 2, the two-dimensional model consists of two rigid legs interconnected individually through a hinge. Each leg contains segmented foot. The mass of the walker is divided into several point masses: hip mass, leg masses, masses of foot without toe, toe masses. Each point mass is placed at the center of corresponding stick. Torsional springs are mounted on both ankle joints and toe joints to represents joint stiffness.

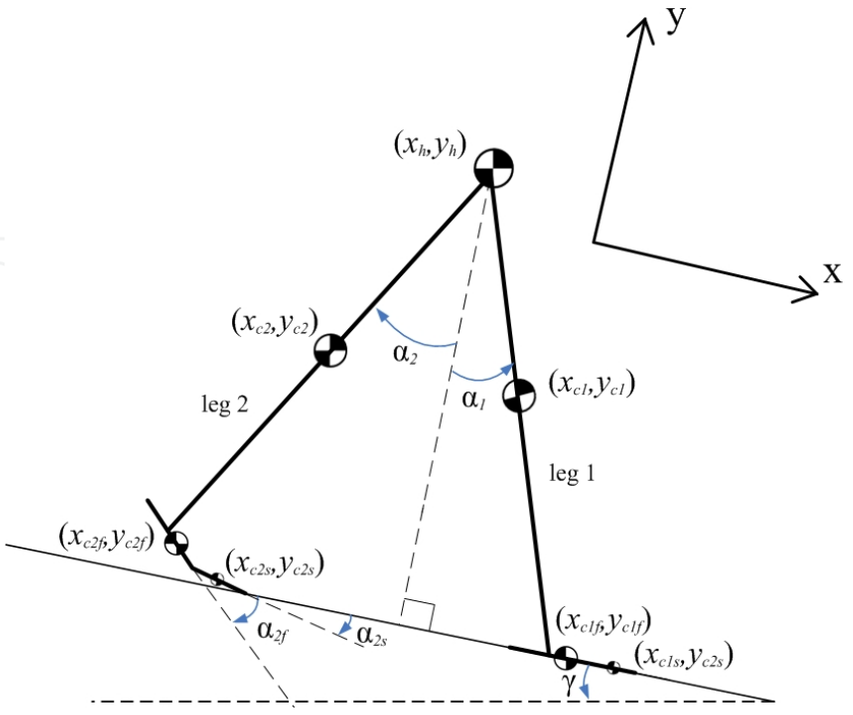

Figure 2. Passivity-based dynamic bipedal walking model with flat segmented feet and compliant ankle joints.

To simplify the motion, we have several assumptions, including that legs suffering no flexible deformation, hip joint with no damping or friction, the friction between walker and ground is enough, thus the flat feet do not deform or slip, and strike is modeled as an instantaneous, fully inelastic impact where no slip and no bounce occurs. The passive walker travels on a flat slope with a small downhill angle.

The process of push-off is dissipated into foot rotation around toe joint and around toe tip, which is the main difference between the passive walking models with rigid flat feet and with segmented flat feet. The toe and foot are restricted into a straight line during the swing phase. When the flat foot strikes the ground, there are two impulses, "heel-strike" and "foot-strike", representative of the initial impact of the heel and the following impact as the whole foot contacts the ground. After foot-strike, the stance leg and the swing leg will be swapped and another walking cycle will begin. The passive walking is restricted to stop in two cases, including falling down and running. We deem that the walker falls down if the angle of either leg exceeds the normal range. The model is considered to running when the stance leg lifts up while the swing foot has not yet contacted the ground. Foot-scuffing at mid-stance is neglected since the model does not include knee joints.

We suppose that the x-axis (hereafter called horizontal coordinate) is along the slope while the y-axis (hereafter called vertical coordinate) is orthogonal to the slope and pointing upwards. The configuration of the walker is defined by the coordinates of the point mass on hip joint and six angles (swing angles between vertical coordinates and each leg, foot angles between horizontal coordinates and each foot, toe angles between horizontal coordinates and each toe), which can be arranged in a generalized vector $q = (x_h, y_h, \alpha_1, \alpha_2, \alpha_{1f}, \alpha_{2f}, \alpha_{1t}, \alpha_{2t})^T$ (see Fig. 2). The positive direction of all the angles are counter-clockwise.

2.3. Walking dynamics

The model can be defined by the rectangular coordinates r, which can be described by the x-coordinate and y-coordinate of the mass points and the corresponding angles (suppose leg 1 is the stance leg):

$$r = [x_h, y_h, x_{c1}, y_{c1}, \alpha_1, x_{c2}, y_{c2}, \alpha_2, x_{c1f}, y_{c1f}, \alpha_{1f}, x_{c2f}, y_{c2f}, \alpha_{2f}, x_{c1s}, y_{c1s}, \alpha_{1s}, x_{c2s}, y_{c2s}, \alpha_{2s}]^T \quad (1)$$

The walker can also be described by the generalized coordinates q as mentioned before:

$$q = [x_h, y_h, \alpha_1, \alpha_2, \alpha_{1f}, \alpha_{2f}, \alpha_{1t}, \alpha_{2t}]^T \quad (2)$$

The definitions of variables mentioned above can be found in Fig. 2.

We defined matrix T as follows:

$$T = \frac{dr}{dq} \quad (3)$$

Thus T transfers the independent generalized coordinates $\dot{q}$ into the velocities of the rectangular coordinates $\dot{r}$. The mass matrix in rectangular coordinates r is defined as:

$$M = diag(m_h, m_h, m_l, m_l, I_l, m_l, m_l, I_l, m_f - m_s, m_f - m_s, I_f, m_f - m_s, m_f - m_s, I_f, m_s, m_s, I_s, m_s, m_s, I_s) \quad (4)$$

Denote F as the active external force vector in rectangular coordinates. The constraint function, which is used to maintain foot contact with ground and detect impacts, is marked as $\xi(q)$. Note that $\xi(q)$ in different walking phases may be different since the contact conditions change.

We can obtain the Equation of Motion (EoM) by Lagrange's equation of the first kind:

$$M_q \ddot{q} = F_q + \Phi^T F_c \quad (5)$$

where F_c is the contact force acted on the walker by the ground to meet the constraint of the stance foot.

$$\xi(q) = 0 \quad (6)$$

where $\Phi = \frac{\partial \xi}{\partial q}$. M_q is the mass matrix in the generalized coordinates:

$$M_q = T^T M T \quad (7)$$

F_q is the active external force in the generalized coordinates:

$$F_q = T^T F - T^T M \frac{\partial T}{\partial q} \dot{q} \dot{q} \quad (8)$$

Equation (6) can be transformed to the following equation:

$$\Phi \ddot{q} = -\frac{\partial (\Phi \dot{q})}{\partial q} \dot{q} \quad (9)$$

Then the EoM in matrix format can be obtained from Equation (5) and Equation (9):

$$\begin{bmatrix} M_q & -\Phi^T \\ \Phi & 0 \end{bmatrix} \begin{bmatrix} \ddot{q} \\ F_c \end{bmatrix} = \begin{bmatrix} F_q \\ -\frac{\partial(\Phi\dot{q})}{\partial q}\dot{q} \end{bmatrix} \tag{10}$$

The equation of strike moment can be obtained by integration of Equation (5):

$$M_q\dot{q}^+ = M_q\dot{q}^- + \Phi^T I_c \tag{11}$$

where $\dot{q}^+$ and $\dot{q}^-$ are the velocities of generalized coordinates after and before the strike, respectively. Here, I_c is the impulse acted on the walker which is defined as follows:

$$I_c = \lim_{t^- \to t^+} \int_{t^-}^{t^+} F_c dt \tag{12}$$

where I_c is the impulse acted on the walker by ground. Since the strike is modeled as a fully inelastic impact, the walker satisfies the constraint function $\xi(q)$. Thus the motion is constrained by the following equation after the strike:

$$\frac{\partial \xi}{\partial q}\dot{q}^+ = 0 \tag{13}$$

Then the equation of strike in matrix format can be derived from Equation (11) and Equation (13):

$$\begin{bmatrix} M_q & -\Phi^T \\ \Phi & 0 \end{bmatrix} \begin{bmatrix} \dot{q}^+ \\ I_c \end{bmatrix} = \begin{bmatrix} M_q\dot{q}^- \\ 0 \end{bmatrix} \tag{14}$$

More detailed description of the bipedal model can be found in [24].

3. Effects of compliant joints and segmented feet

Based on the EoMs mentioned above, we analyze the effects of compliant ankles and toes on energetic efficiency and stability of dynamic bipedal walking. All masses and lengthes are normalized by the leg mass and leg length respectively. The spring constants (stiffness of ankle joint and toe joint) are normalized by both the mass and the length of leg.

3.1. Energetic efficiency

Energetic efficiency is an important gait characteristics. The energy consumption of passive dynamic based models is usually represented in the nondimensional form of ”specific resistance”: energy consumption per kilogram mass per distance traveled per gravity [8]. However, for passive walkers on a gentle slope, specific resistance is not a suitable measure of efficiency, since all walkers have the same specific resistance for a given slope [12]. Therefore, similar to [12], normalized walking velocity is used as the measure of efficiency, such that ”most efficient” is synonymous of ”fastest”.

The walking velocity of the rigid foot model (without toe joints) decreases monotonically as foot length or foot ratio (the ratio of distance between heel and ankle joint to distance between ankle joint and toe tip) grows (see Fig. 3(a)). For the segmented foot model, the walker moves slower for longer foot according to the main tendency (see Fig. 3(b)). Walking velocity achieves the maximum value when foot ratio is near 0.3 for any fixed foot length.

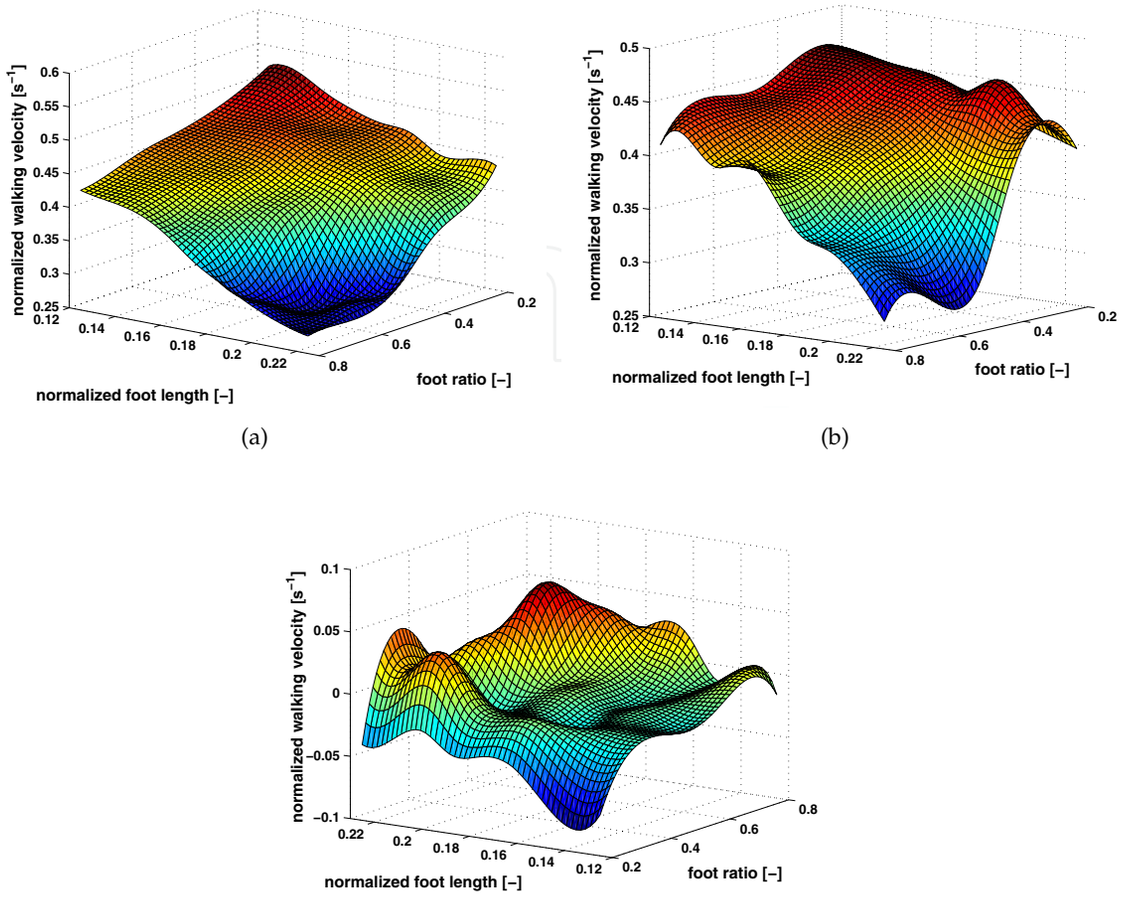

Figure 3. Comparison of walking velocities of rigid foot model and segmented foot model. The curved surfaces are smooth processed based on the sample data. (a) Average walking velocity versus foot length and foot ratio for rigid flat-foot passive walking model. (b) Average walking velocity versus foot length and foot ratio for segmented flat-foot passive walking model. (c) The difference of walking velocity of the two models, obtained from (b) subtracted by (a). Both walking velocity and foot length are normalized by leg length. Foot ratio is defined as the ratio of distance between heel and ankle joint to distance between ankle joint and toe tip.

A peak appears at relative large foot length (larger than 0.2) and foot ratio near 0.3, which is similar to the foot structure of human beings [25]. The comparison of the two models shows that the walker with segmented feet moves slower than rigid foot model with small foot length, however, the velocity of segmented foot model is larger when the foot is long enough, especially when foot ratio is near 0.3. In another word, if the segmented foot ratio is close real human foot, the segmented foot model is more efficient than the rigid foot model.

3.2. Walking stability

We evaluate adaptive walking of the model on uneven terrain to analyze the walking stability. Figure 4 shows the relationship between the maximal allowable ground disturbance (a step down) the walker can overcome and the foot ratio of rigid foot bipedal model. The maximal allowable ground disturbance decreases monotonically as the foot ratio grows, which is

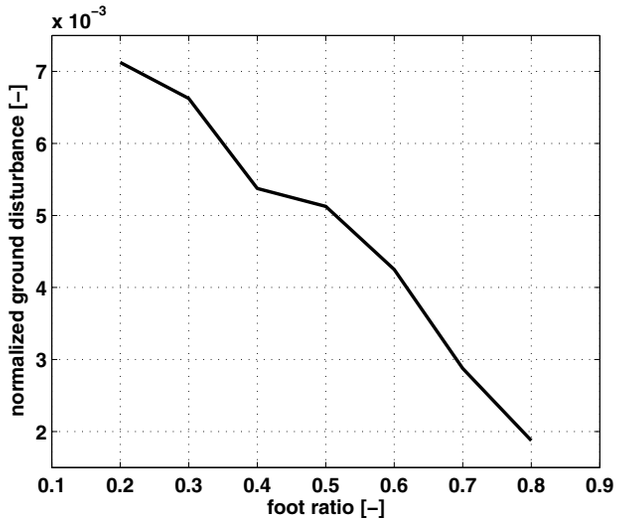

Figure 4. Adaptability of the rigid foot model with different foot ratios. The normalized foot length is 0.1875. The ground disturbance is also normalized by leg length.

similar to the trend of walking velocity. In case of short hindfoot and long forefoot (foot ratio is 0.2), the walker can return to stable motion cycle after a ground disturbance larger than 0.7 percent of leg length. However, the maximum disturbance the model can overcome decreases below 0.2 percent of leg length when the lengths of hindfoot and forefoot are comparable (foot ratio is 0.8). The relationship between the maximal allowable ground disturbance and foot ratio of segmented foot model also shows a great resemblance to the trend of walking velocity (Fig. 5 shows the results). The maximum value is obtained when the foot ratio is 0.3.

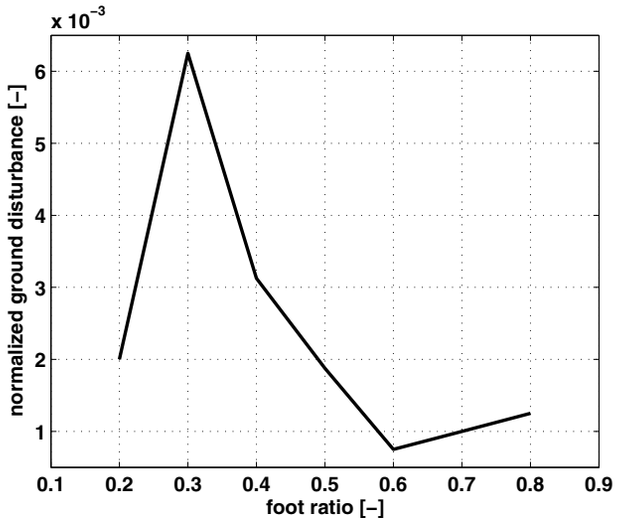

Figure 5. Adaptability of the segmented foot model with different foot ratios. The normalized foot length is 0.1875. The ground disturbance is also normalized by leg length.

In that case the model can overcome ground disturbance larger than 0.6 percent of leg length. The adaptability of the segmented foot model decreases significantly if the foot ratio changes to other values. The results indicate that there exists a best foot structure of the segmented foot model, which achieves both excellent adaptability and walking velocity.

From the analysis above, one can find that the segmented foot model has comparable walking adaptability with rigid foot models in the case of suitable foot ratios. However, the walkers with segmented feet perform worse in other cases.

4. Applications to prosthesis and exoskeleton

The theoretical analysis mentioned above indicates that the segmented foot model with compliant joints is more complicated than the rigid foot model in both foot structure and walking sequence. However, segmented foot models with foot structure close to human body show better walking performance (energetic efficiency and stability) compared with rigid-foot walking. Based on the results, here we introduce the design of the lower-limb prosthesis (PANTOE 1) [26] and exoskeleton prototype (EXO-PANTOE 1) [27] with compliant joints and segmented foot. At first, a brief overview of compliant actuators in robotics is presented. It shows the reasons of using spring based compliant actuators for joints in the proposed prosthesis and exoskeleton.

4.1. Compliant actuators in joints

In practice, a combination of sophisticated nonlinear control strategies and analytical methods is required to deal with the uncontrollable and underactuated degrees of freedom introduced by joint compliance. As a result, many robotic applications have used stiff actuation schemes and high-stiffness materials. However, mechanically compliant systems, such as elastic joints, may be used for shock absorbtion and be exploited to store energy and decrease control complexity. As a new trend in robotics, various kinds of compliant actuators and compliant joints have been introduced to real robot applications, for instance, hexapod robot [28], quadruped system [29] and bipedal walking [30].

According to the composition of the elastic elements, compliant actuators can be roughly divided into several main classes. The first category is the spring based compliance. The well-known examples are the Series Elastic Actuators (SEA) developed by Pratt and Williamson [31] and the two-legged robot Spring Flamingo [32]. Starting from the Series Elastic Actuators, various legged robot applications have been equipped with motor-spring systems. Yamaguchi *et al* [33] used a non-linear spring mechanism to make predefined changes in stiffness of biped robot possible. Meyer *et al* [34] described a simple and low-cost humanoid leg with compliant joints and springy feet, aiming for a repetitive jumping system. Hurst *et al* [35] designed the Actuator with Mechanically Adjustable Series Compliance (AMASC) which consists of a drive motor connected in series with a pair of large, variable stiffness springs. Van Ham *et al* [36] reported a controlled passive walker Veronica actuated with the Mechanically Adjustable Compliance and Controllable Equilibrium Position Actuator (MACCEPA) which uses a dedicated servo motor and solid springs to control the compliance and equilibrium position.

Another category is the pneumatic artificial muscles based compliance. The well-known artificial muscles in the field of dynamic walking are the pneumatic McKibben muscles [37]. In addition, the Pleated Pneumatic Artificial Muscle (PPAM) designed by [38], has been successfully implemented in the biped Lucy [30]. However, such air muscles based mechanisms may be the barrier that constrains the dynamic walking systems, especially the lower-limb prostheses and exoskeletons, in practical use. One of the disadvantages is that with air muscles, it is difficult to perform precise control. Other problems, for example, include the use of compressed air and the inefficient down-regulation of pressure of the onboard

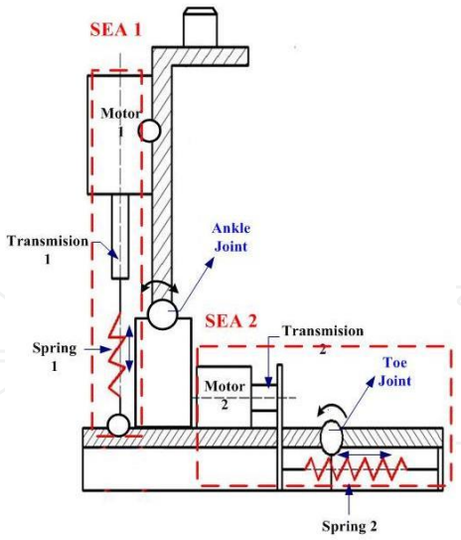

Figure 6. Schematics diagram of the segmented foot with compliant joints. The two main components of the prosthesis are two SEAs, which are used to drive the ankle and toe joints respectively.

air storage system. Thus, several recent studies try to change air muscles into motor-spring systems as compliant actuators for dynamic walking systems, e.g. [39].

In addition, there are other types of compliant actuators in robotics. For example, shape memory alloys show impressive actuation characteristics, while suffer from slow response and motion constraints [40]. Other interesting compliant actuators include artificial muscle actuator using fluid [41], polymer materials [42], dielectric elastomers [43], etc. Most of them are used in particular environments and difficult to implement in autonomous systems, especially in lower-limb prostheses and exoskeletons.

As mentioned above, currently, spring based compliance is the most promising compliant actuators in the field of dynamic walking. By using the proper spring based elastic mechanisms, lower-limb prostheses and exoskeletons may be capable of performing stable walking on different terrains and with controllable walking velocity. Applying compliant actuators to lower-limb rehabilitation systems provides not only new challenges for bipedal locomotion but also improvement of practical use.

4.2. Powered ankle and toe with compliant actuators

As discussed above, we finally used two series elastic actuators (SEA) to construct ankle and toe joints. Each SEA includes a DC motor, a transmission and a spring structure. Compared with other actuators, SEA has several benefits: 1) the actuator exhibits lower output impedance and back-driveability; 2) shock tolerance is greatly improved by the spring placed in series between the transmission and the load; 3) the motor's required force is reduced; 4) force control stability is improved, even in intermittent contact with hard surfaces; 5) energy can be stored and released in the elastic element, potentially improving efficiency [31, 45]. The design of the two SEAs will be introduced in details in the following part of the paper.

The design of the powered joints is based on the functionality of human toe and ankle joints. As shown in Fig. 6, the basic architecture of the segmented foot is an integration of two SEAs, which are used to drive the ankle and toe joints respectively. Each SEA comprises a DC motor, a ball screw transmission and a spring structure. Because human toe joint only outputs net positive work at the moment TO, the toe joint is designed to rotate counterclockwise passively,

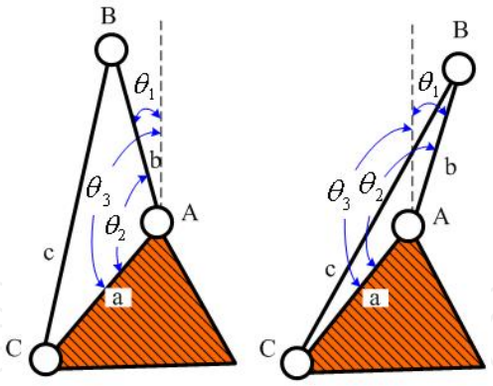

Figure 7. The ankle joint can be simplified as a special three-bar mechanism, of which the length of c can be modulated by SEA 1.

and to rotate clockwise actively. When toe joint is forced to rotate counterclockwise, Spring 2 will be extended to store energy. At the moment TO, Spring 2 will release the stored energy and Motor 2 will drive the toe joint to rotate clockwise via Transmission 2 and Spring 2. Spring 2 comprises four drawsprings set in parallel and the stiffness is $200N/cm$. Motor 2 used in the current design is a $30W$ DC motor with an angle encoder.

The functionality of the human ankle joint can be realized by a special three-bar mechanism, shown in Fig.10. The special three-bar mechanism comprises three bars (a, b and c) and three hinges (A, B and C). Hinge A is the ankle joint. Bars a and b are the foot and the shank respectively. c is a special bar, of which the length can be regulated by SEA 1. θ_1 is the angle of the ankle joint, which is used to control the movement of the ankle. θ_1 can be calculated by the following equation:

$$\theta_1 = \arccos \frac{L_a^2 + L_b^2 - L_c^2}{2L_a L_b} - \theta_3 \tag{15}$$

where L_a, L_b and L_c are the length of the bars a, b and c respectively. L_a and θ_3 can be calculated by L_3 and H_1:

$$\theta_3 = \pi - \arctan \frac{L_3}{H_1} \tag{16}$$

$$L_a = \sqrt{L_3^2 + H_1^2} \tag{17}$$

where L_3 is the level distance of the ankle joint from the end of the heel and H_1 is the height of the ankle joint from the ground. L_c is determined by SEA 1. When Spring 1 is compressed or pulled by Transmission 1 (the nut of the ball screw, Nut 1, move upward), the L_c becomes shorter. When Spring 1 is extended or pushed by Transmission 1 (Nut 1 move downward), the length of c becomes longer. In fact, the state of Spring 1 and the movement of Transmission 1 are not independent, namely, L_c is determined by a combined motion of Spring 1 and Transmission 1. L_c can be obtained by the following equation.

$$L_c = L_s + L_t + \frac{F}{K_1} + \Delta_1 \tag{18}$$

Where L_s is the length of Spring 1 with no load. L_t is the length of Transmission 1 with the nut at the initial position; F is the load on Spring 1, which is determined by the weight of the subject and the walking state; K_1 is the spring stiffness of Spring 1. Δ_1 is the displacement of the nut of Transmission 1.

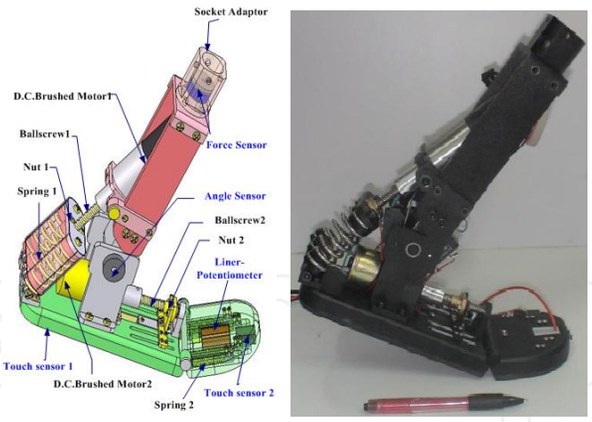

(a) (b)

Figure 8. The CAD model and the prototype of PANTOE 1 with compliant joints and segmented foot. The prototype is made of aluminium-alloy. The weight is 1.47 kg (not including the Li rechargeable battery about 1 kg), comparable to the weight of the subject's limb. The full angles of the ankle and the toe joints are 45^o and 90^o respectively.

4.3. Powered prosthesis with segmented foot

PANTOE 1 is short for foot-prosthesis with Powered Ankle and Toe Joints. Our aim is to build an ankle-foot prosthesis with compliant powered joints and segmented foot to replicate the functionality of human foot as closely as possible. SEA 1 was designed based on the angle range of θ_1 from -16^o to 27^o. Spring 1 was constructed with three springs placed together in parallel. The stiffness of Spring 1 is about $500N/cm$. The pitch of the ball screw Transmission 1 is $4mm$ per revolution, then the nut is self-locking. Because the ankle needs to provide high power output to propel the body, we chose a $83W$ FAULHABER brushed DC motor (with rotary encoder) as Motor 1. Figure 8 shows the CAD model and the prototype of PANTOE 1 in detail. In order to decrease the total weight, PANTOE 1 is made of aluminium-alloy. This design weighs $1.47kg$, not including the rechargeable Li battery and the molded socket.

4.4. Lower-limb exoskeleton with segmented foot

EXO-PANTOE 1 is short for below-knee exoskeleton with powered ankle and toe joints. It is designed for a subject suffering from some ankle pathology. The information of the subject is shown in Table 1. Figure 9 shows the CAD model and the prototype of EXO-PANTOE 1 in

Parameter	Value
length of the foot L_1	$265mm$
length of the forefoot L_2	$79mm$
level distance of the ankle joint from the end of the heel L_3	$68mm$
height of the ankle joint from the ground H_1	$83mm$
maximal plantar flexion angle of the ankle joint θ_p	27°
maximal dorsiflexion angle of the ankle joint θ_d	16°
maximal angle of the toe joint θ_t	90°

Table 1. Information of the subject.

detail. The design concept of EXO-PANTOE 1 is similar to PANTOE 1. Two SEAs are used to drive the ankle and toe joints respectively.

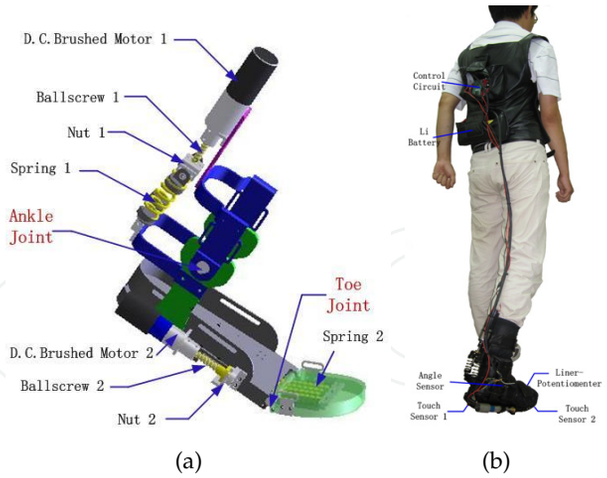

Figure 9. The CAD model and the prototype of EXO-PANTOE 1 with compliant joints and segmented foot. The prototype is made of aluminium-alloy. The weight is 1.2kg (not including the Li rechargeable battery about 0.5kg), acceptable to the subject. The full angles of the ankle and the toe joints are 45^o and 90^o respectively.

4.5. Sensors and control

Sensors and control method used in PANTOE 1 and EXO-PANTOE 1 are similar. The sensor system includes two touch sensors, a angle sensors, a linear-potentiometer and a force sensor. The reactions between the ground and the foot are detected by touch sensors 1 and 2. The angle sensor is used to measure the rotation angle of the ankle joint. Assembled in parallel with series Spring 2 (see Fig. 9(a)), the linear-potentiometer is utilized to measure the rotation angle of the toe joint and the force of the Spring 2 at the same time. The force between the subject and the system is measured by the force sensor.

For gait identification, we divide the walking gait cycle into seven phases. Each phase represents a unique state where the system will be controlled by a specific control strategy and perform a specific behavior. Besides, a state can switch to one another if the triggering transition requirements are meet. This method can be called finite-state control and can be describe as follows [46]:

$$A_i = f_a(S_i) \tag{19}$$

where f_a is the action function indicating the specific output behavior A_i of the specific state S_i.

$$S_{i+1} = f_s(S_i, I_i) \tag{20}$$

where f_s is the transition function indicating the transition between two adjacent states and I_i represents the input triggering information.

As described, a level ground walking gait cycle begins with the heel strike of one foot and ends with the next heel strike of the same foot [20]. It is generally divided into the stance phase when the foot is on the ground and the swing phase when the foot is off the ground. To get a more accurate description of the prosthesis state, we divide each phase into different sub-phases:

1) Stance Phase:

Controlled plantar flexion of ankle (CPA): CPA begins at heel-strike when the ankle joint begins to plantar flex and ends at foot-flat when toe-strike occurs. The behavior of the ankle

joint at this state is consistent with a linear spring response since the output joint torque is proportional to the joint angle.

Controlled dorsiflexion of ankle (CDA): CDA begins at foot-flat when the ankle joint begins to dorsiflex and ends when the ankle reaches the maximum dorsiflexion angle. The behavior of the ankle joint at this state can be described as a nonlinear spring.

Powered plantar flexion of ankle (PPA): PPA begins after CDA when the ankle joint begins to plantar flex again and ends at the instant of toe-off. The function of the ankle joint at this state is the superposition of a nonlinear spring and a torque source. This phase is the main phase that can reflects the dynamical characteristics of the ankle joint.

Controlled dorsiflexion of toe (CDT): CDT begins after heel-off when the toe joint is compressed and begin to plantar flex. It ends when the toe joint is compressed to specific extent. The behavior of the toe joint at this state can be modeled as a linear spring.

Powered plantar flexion of toe (PPT): PPT begins when the toe joint angle reaches a specific value and the toe joint begins to dorsiflex to push the body forward and upward together with the ankle joint. It ends at toe-off. The toe joint's behavior at this state can be modeled as the superposition of a linear spring and a torque source.

2) Swing Phase:

Early swing (ESW): ESW begins at toe-off when the ankle joint and the toe joint begin to return to the equilibrium position and ends after a predefined time period when the two joints have reached back to the equilibrium position. Both of the two joints play the role of position source to reset the prosthesis to equilibrium position.

Late swing (LSW): LSW begins just after the ESW and ends at the next heel-strike. The toe joint and the ankle joint just keep the balanced state and get ready for the beginning of the next gait cycle. The function of the two joints can also be modeled as a position source.

Figure 10 shows the finite-state control scheme for level-ground walking with segmented foot. We define the ankle joint angle to be zero when the shank is perpendicular to the foot. From the zero position, the angle will be negative if the ankle plantar flexs and positive if the ankle dorsiflexs. The toe joint angle is defined to be zero when the joint is not compressed and to be positive we compressed to dorsiflex. To accurately identify each gait state and decide the transition between different states, we collect the information below: a) Heel contact (H), $H=0$ indicates that the heel is off the ground and vice versa; b) Heel pressure (F_H), F_H indicates the pressure that the ground exerts to the heel; c) Toe contact (T), $T=0$ indicates that the toe is off the ground and vice versa; d) Toe pressure (F_T), F_T indicates the pressure that the ground exerts to the toe; e)Ankle joint angle (θ_a); f) Ankle joint's angular velocity ($\dot{\theta}_a$), $\dot{\theta}_a$ indicates the rotatory direction of the ankle joint; g) Toe joint angle (θ_t); h) Ankle torque (T_a); i) Stance phase time period (Δt_{stance}), Δt_{stance} can be used as an indicator of the walking speed; j) Swing phase time period (Δt_{swing}), Δt_{swing} can be used as an indicator of the walking speed. Figure 11 shows the hardware of the proposed control platform.

5. Experimental results

5.1. Walking performance

For PANTOE 1, we have done several preliminary experiments to evaluate the functionality of the prototype. The amputee subject was 45 years of age, 1.70m in height and 71kg in weight.

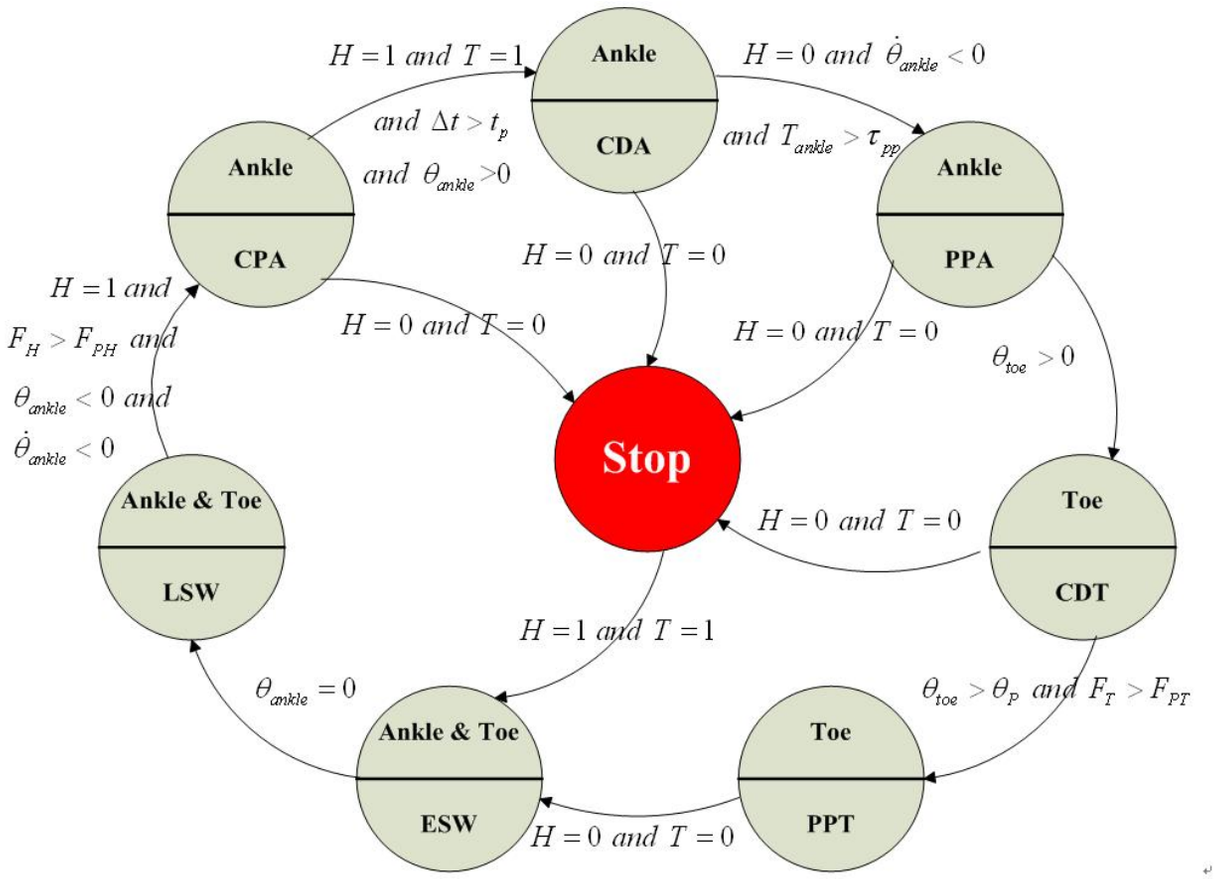

Figure 10. Finite-state control for level-ground walking with segmented foot.

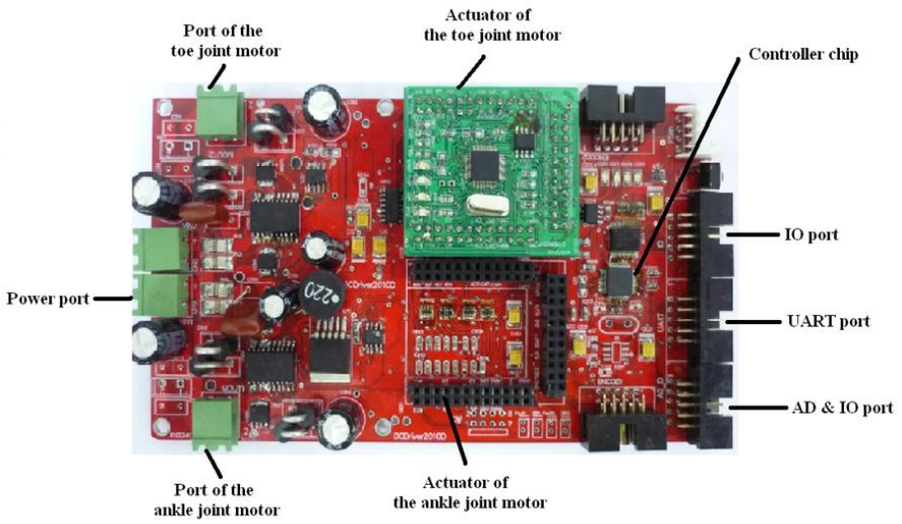

Figure 11. The hardware of the control platform.

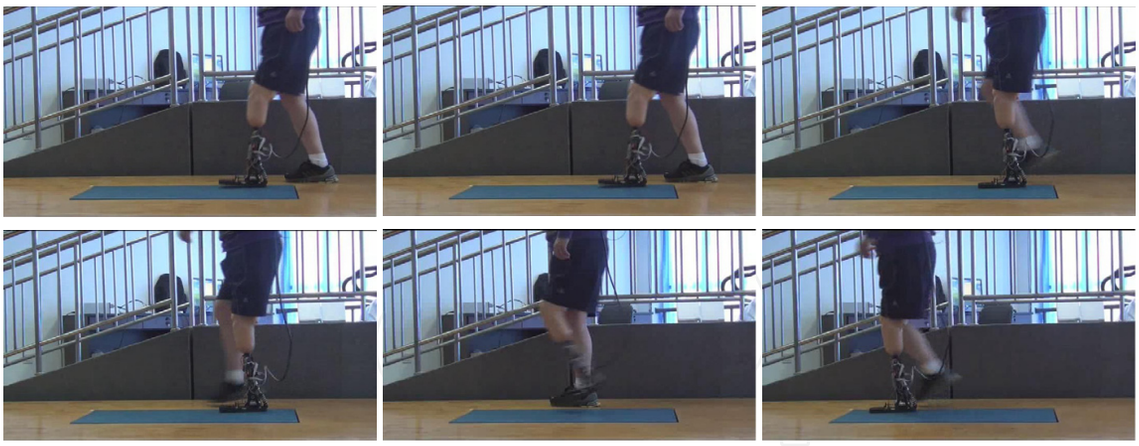

Figure 12. A sequence of photos captured during walking of the amputee subject.

He wore the proposed prosthesis during the experiment. The ratio between the length of the residual shank (the distance between patella to the amputated site) to that of the sound shank (measured from patella to malleolus lateralis) is 0.4m. Fig. 12 shows the walking performance.

EXO-PANTOE 1 is worn by a subject whose right ankle is injured and can not output sufficient power during walking. With the powered ankle and toe joints, EXO-PANTOE 1 is able to provide enough energy to the subject and help him relearn the normal walking gait (shown in Fig. 13).

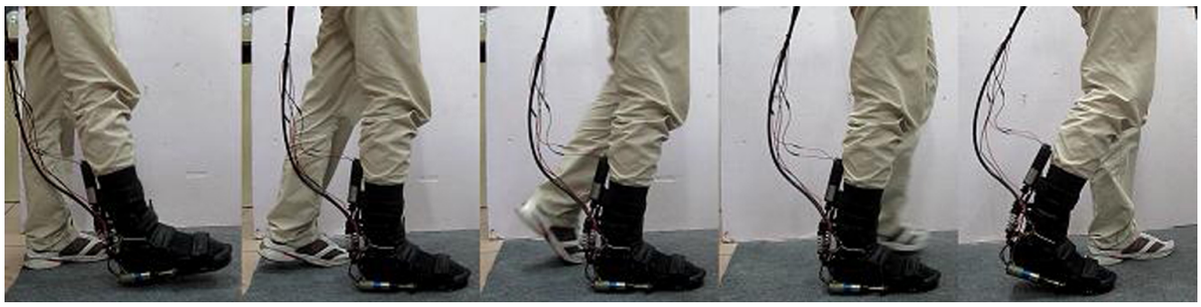

(a) Stance phase

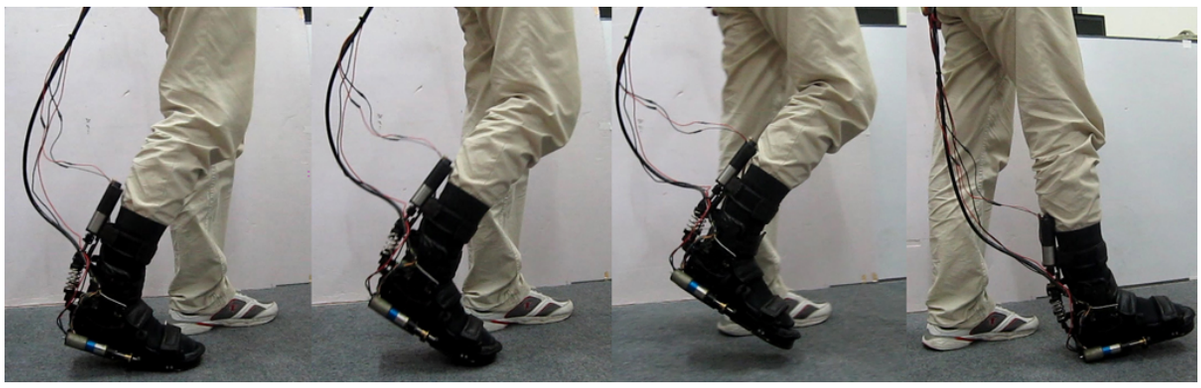

(b) Swing phase

Figure 13. Sequence pictures captured from the walking motion of the subject wearing EXO-PANTOE 1 in a walking gait cycle beginning with heel-strike. The result indicates that EXO-PANTOE 1 can assist the subject relearn the human walking gait.

5.2. Energy consumption

In order to analyze the effects of the segmented foot structure on the energetic efficiency during walking, we have measured the energy consumption of EXO-PANTOE 1 during the subject walking at his most comfortable speed ($1.1m/s$) in three cases. In the first case, the segmented foot is locked with a mechanical structure and the foot just acts as a single rigid plate. In the second case, Motor 2 does not work at all and the toe joint can only be bent passively. In the third case, the toe joint is active and it is able to output sufficient net positive work to the subject during the TO phase. In these three cases, the ankle joint always provides enough energy to the subject. Before the measurement of the energy consumption, in each case the subject is allowed to have a long enough training period to adapt to the exoskeleton.

As shown in Fig. 14, one can find that EXO-PANTOE 1 consumes the most energy in the first case (see Fig. 14(a)), which indicates that the segmented foot plays important role in improving energetic efficiency. The total energy consumed in the second case and the third case is close, where the segmented foot with active toe performs slightly better (see Fig. 14(b)

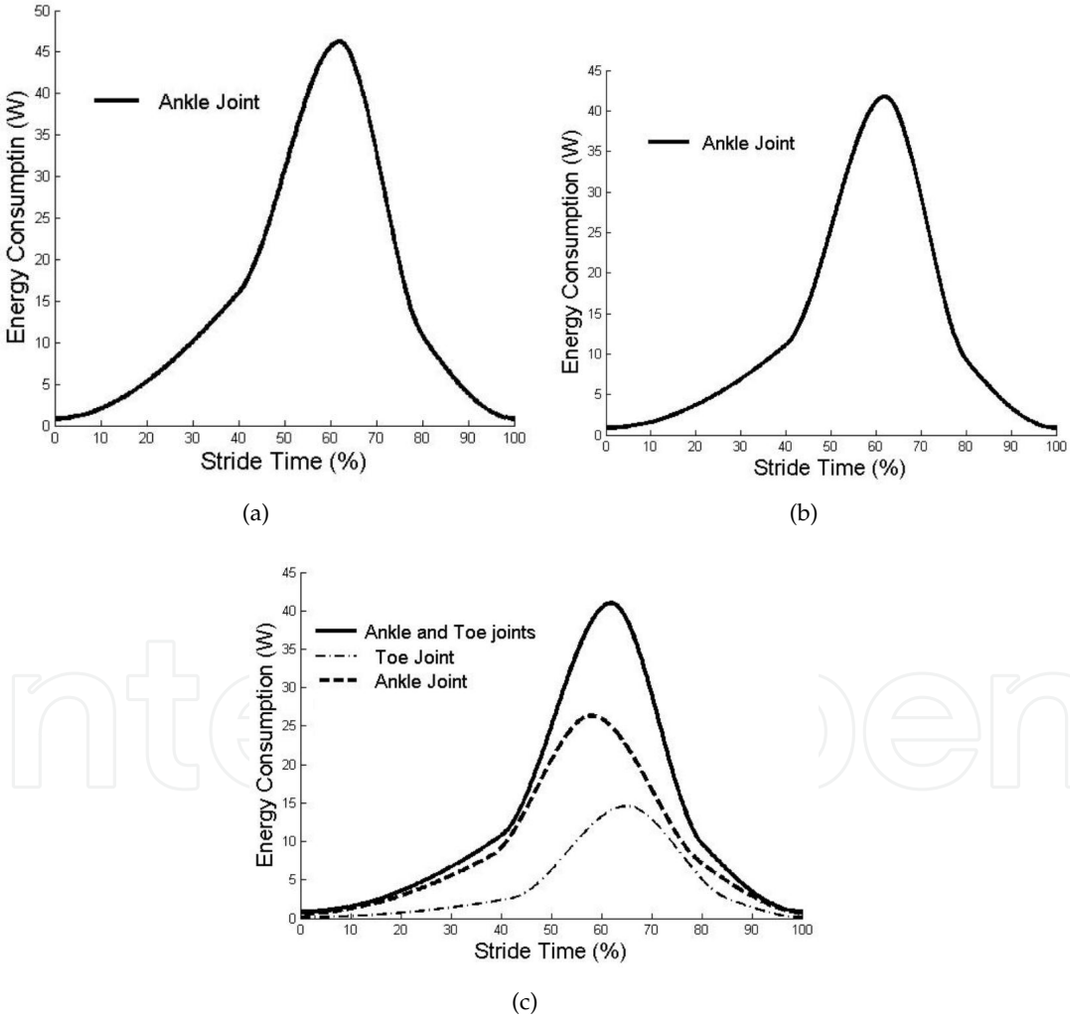

Figure 14. Energy consumption of EXO-PANTOE 1 in one stride cycle. (a)Energy consumption of EXO-PANTOE 1 when the foot is a single rigid plate. (b) Energy consumption of EXO-PANTOE 1 when the toe joint can only be bent passively. (c)Energy consumption of EXO-PANTOE 1 when the toe joint can output sufficient power.

and Fig. 14(c)). The ankle joint in the third case consumes much less energy than that in the second case. The result shows that powered toe joint can share the energy cost of the ankle joint, and enables the development of more efficient and effective powered lower-limb exoskeleton.

Acknowledgements

This work was supported by the National Natural Science Foundation of China (No. 61005082, 61020106005), Doctoral Fund of Ministry of Education of China (No. 20100001120005), PKU-Biomedical Engineering Joint Seed Grant 2012 and the 985 Project of Peking University (No. 3J0865600).

Author details

Qining Wang, Jinying Zhu, Yan Huang, Kebin Yuan and Long Wang
Intelligent Control Laboratory, College of Engineering, Peking University, Beijing 100871, China
Beijing Engineering Research Center of Intelligent Rehabilitation Engineering, Beijing 100871, China

6. References

[1] Carson M. C, Harrington M. E, Thompson N, O'Connor J. J, Theologis T. N (2001) Kinematic analysis of a multi-segment foot model for research and clinical applications: a repeatability analysis. J. Biomech. 34, 1299–1307.
[2] MacWilliams B. A, Cowley M, Nicholson D. E (2003) Foot kinematics and kinetics during adolescent gait. Gait Posture 17, 214–224.
[3] Myers K. A, Wang M, Marks R. M, Harris G. F (2004) Validation of a multisegment foot and ankle kinematic model for pediatric gait. IEEE T. Neur. Sys. Reh. 12(1), 122–130.
[4] Okita N, Meyers S. A, Challis J. H, sharkey N. A (2009) An objective evaluation of a segmented foot model. Gait Posture 30, 27–34.
[5] Nishiwakiz K, Kagamiy S, Kuniyoshiz Y, Inabaz M, Inouez H (2002) Toe joints that enhance bipedal and fullbody motion of humanoid robots. Proceedings of IEEE International Conference on Robotics and Automation, pp. 3105–3110.
[6] Sellaouti R, Stasse O, Kajita S, Yokoi K, Kheddar A (2006) Faster and smoother walking of humanoid hrp-2 with passive toe joints. Proceedings of IEEE/RSJ International Conference on Intelligent Robots and Systems, pp. 4909–4914.
[7] Hirai K, Hirose M, Haikawa Y, Takenaka T (1998) The development of the Honda humanoid robot. Proceedings of IEEE International Conference on Robotics and Automation, pp. 1321–1326.
[8] Collins S, Ruina A, Tedrake R, Wisse M (2005) Efficient bipedal robots based on passive-dynamic walkers. Science 307, 1082–1085.
[9] McGeer T (1990) Passive dynamic walking. Int. J. Robot. Res. 9, 68–82.
[10] Mochon S, McMahon T. A (1980) Ballistic walking. J. Biomech. 13(1), 49–57.
[11] Ruina A, Bertram J. E. A, Srinivasan M (2005) A collisional model of the energetic cost of support work qualitatively explains leg sequencing in walking and galloping, pseudo-elastic leg behavior in running and the walk-to-run transition. J. Theor. Biol. 237(2), 170–192.
[12] Kwan M, Hubbard M (2007) Optimal foot shape for a passive dynamic biped. J. Theor. Biol. 248, 331–339.
[13] Hobbelen D. G. E, Wisse M (2008) Ankle actuation for limit cycle walkers. Int. J. Robot. Res. 27, 709–735.

[14] Wang Q, Huang Y, Wang L (2010a) Passive dynamic walking with flat feet and ankle compliance. Robotica 28, 413–425.
[15] Wang Q, Huang Y, Zhu J, Wang L, Lv D (2010b) Effects of foot shape on energetic efficiency and dynamic stability of passive dynamic biped with upper body. Int. J. Hum. Robot. 7(2), 295–313.
[16] Kumar R. P, Yoon J, Christiand, Kim G (2009) The simplest passive dynamic walking model with toed feet: a parametric study. Robotica 27, 701–703.
[17] Klute G. K, Czerniecki J, Hannaford B (1998) Development of powered prosthetic lower limb. The 1st Natl. Meeting, Veterans Affairs Rehabil. R and D service.
[18] Versluys R, Peeraer L, Van der Perre G, Van Gheluwe B, Lefeber D (2007) Design of a powered below-knee prosthesis. The 12th World Congr. Int. Soc. Prosthet. Orthot., 2007.
[19] Versluys R, Desomer A, Lenaerts G, Van Damme M, Bey P, Van der Perre G, Peeraer L, Lefeber D (2008) A pneumatically powered below-knee prosthesis: design specifications and first experiments with an amputee. Proceedings of the 2nd IEEE/RAS-EMBS International Conference on Biomedical Robotics and Biomechatronics, pp. 372–377.
[20] Au S. K, Weber J, Herr H (2009) Powered ankle-foot prosthesis improves walking metabolic economy. IEEE Trans. Robot. 25(1), 51–66.
[21] Dollar A. M, Herr H (2008) Lower extremity exoskeletons and active orthoses: challenges and state-of-the-art. IEEE Trans Robot. 24(1), 144–158.
[22] Chu A, Kazerooni H, Zozz A (2005) On the biomimetic design of the Berkeley Lower Extremity Exoskeleton (BLEEX). Proceedings of the IEEE International Conference on Robotics and Automation, pp. 4345–4352.
[23] Hayashi T, Kawamoto H, Sankai Y (2005) Control method of robot suit HAL working as operator's muscle using biological and dynamical information. Proceedings of the IEEE/RSJ International Conference on Intelligent Robots and Systems, pp. 3063–3068.
[24] Huang Y, Wang Q, Gao Y, Xie G (2012) Modeling and analysis of passive dynamic bipedal walking with segmented feet and compliant joints. Acta Mechanica Sinica. (accepted)
[25] Wang W. J, Crompton R. H (2004) Analysis of the human and ape foot during bipedal standing with implications for the evolution of the foot. J. Biomech. 37, 1831–1836.
[26] Zhu J, Wang Q, Wang L (2010) PANTOE 1: Biomechanical design of powered ankle-foot prosthesis with compliant joints and segmented foot. Proceedings of the IEEE/ASME International Conference on Advanced Intelligent Mechatronics, pp. 31–36.
[27] Zhu J, Wang Q, Huang Y, Wang L (2011) Adding compliant joints and segmented foot to bio-inspired below-knee exoskeleton. Proceedings of the IEEE International Conference on Robotics and Automation, pp. 605–610.
[28] Saranli U, Buehler M, Koditschek D (2001) RHex: A simple and highly mobile hexapod robot. Int. J. Robot. Res. 20(7), 616–631.
[29] Poulakakis I, Papadopoulos E, Buehler M (2006) On the stability of the passive dynamics of quadrupedal running with a bounding gait. Int. J. Robot. Res. 25(7), 669–687.
[30] Vanderborght B, Verrelst B, Van Ham R, Lefeber D (2006) Controlling a bipedal walking robot actuated by pleated pneumatic artificial muscles. Robotica. 24, 401–410.
[31] Pratt G. A, Williamson M (1995) Series elastic actuators. Proceedings of the IEEE International Conference on Intelligent Robots and Systems, pp. 399–406.
[32] Pratt J (2000) Exploiting inherent robustness and natural dynamics in the control of bipedal walking robots, Ph.D. Thesis, Computer Science Department, MIT, Cambridge, MA.
[33] Yamaguchi J, Nishino D, Takanishi A (1998) Realization of dynamic biped walking varying joint stiffness using antagonistic driven joints. Proceedings of the IEEE International Conference on Robotics and Automation, pp. 2022–2029.

[34] Meyer F, Spröwitz A, Lungarella M, Bettbouze L (2004) Simple and low-cost compliant leg-foot system. Proceedings of the IEEE/RSJ International Conference on Intelligent Robots and systems, pp. 515–520.
[35] Hurst J. W, Chestnutt J. E, Rizzi A. A (2004) An actuator with physically variable stiffness for highly dynamic legged locomotion. Proceedings of the IEEE International Conference on Robotics and Automation, pp. 4662–4667.
[36] Van Ham R, Vanderborght B, Verrelst B, Van Damme M, Lefeber D (2006) Controlled passive walker Veronica powered by actuators with independent control of equilibrium position and compliance. Proceedings of the IEEE International Conference on Humanoids, pp. 234–239.
[37] Caldwell D, Medrano-Cerda G, Goodwin M (1995) Control of pneumatic muscle actuators. IEEE Control Syst. Mag. 15(1), 40–48.
[38] Daerden F, Lefeber D (2001) The concept and design of pleated pneumatic artificial muscles. Int. J. Fluid Power 2(3), 41–50.
[39] Wisse M, Schwab A. L, van der Linde R. Q, van der Helm F. C. T (2005) How to keep from falling forward: elementary swing leg action for passive dynamic walkers. IEEE Trans. Robot. 21(3), 393–401.
[40] Choi S. B, Han Y. M, Kim J. H, Cheong C. C (2001) Force tracking control of a flexible gripper featuring shape memory alloy actuators. Mechatronics 11, 677–690.
[41] Boblan I, Bannasch R, Schwenk H, Prietzel F, Miertsch L, Schulz A (2004) A human-Like robot hand and arm with fluidic muscles: biologically inspired construction and functionality. Lecture Notes in Artificial Intelligence 3139, 160–179.
[42] Kornbluh R, Pelrine R, Eckerle J, Joseph J (1998) Electrostrictive polymer artificial muscle actuators. Proceedings of the IEEE International Conference on Robotics and Automation, pp. 2147–2154.
[43] Wissler M, Mazza E (2007) Electromechanical coupling in dielectric elastomer actuators. Sensers and Actuators A - Physical 138(2), 384–393.
[44] Inman V. T, Ralston H. J, Todd F (1981) Human Walking, Baltimore, MD: Williams and Wilking.
[45] Robinson D (2000) Design and an analysis of series elasticity in closed-loop actuator force control. Ph.D. Thesis, MIT.
[46] Zlatnik D, Steiner B, Schweitzer G (2002) Finite-state control of a trans-femoral prosthesis. IEEE Trans. Control Syst. Technol. 10(3), 408–420.